Reflectance Spectroscopy of 27 Fine-particulate Mineral Samples from Far-ultraviolet through Mid-infrared (0.12–20 μm)

Melissa D. Lane[1] , Edward A. Cloutis[2] , Roger N. Clark[3] , M. Darby Dyar[3,4] , Joern Helbert[5] , Amanda R. Hendrix[3] ,
Gregory Holsclaw[6] , Alessandro Maturilli[5] , Neil Pearson[3] , Mikki Osterloo[7] , Faith Vilas[3] , and Daniel Applin[2]

[1] Fibernetics LLC, Lititz, PA, USA; lane@fibergyro.com
[2] University of Winnipeg, Winnipeg, Canada
[3] Planetary Science Institute, Tucson, AZ, USA
[4] Mount Holyoke College, South Hadley, MA, USA
[5] Deutsches Zentrum für Luft- und Raumfahrt, Berlin, Germany
[6] University of Colorado Boulder, Boulder, CO, USA
[7] Space Science Institute, Boulder, CO, USA
Received 2023 August 19; revised 2024 May 30; accepted 2024 May 30; published 2024 August 28

Abstract

This paper presents far-ultraviolet through mid-infrared (0.12–20 μm) reflectance spectra of 27 fine-particulate (<10 μm) terrestrial mineral samples, providing continuous spectra that cover an unusually broad spectral range and are of unusually fine particle size relative to most existing spectral libraries. These spectra of common geologic materials are useful for future applications that study the dust on various planetary bodies. Reflectance spectra were acquired of the samples at multiple laboratories at multiple wavelengths. All of the spectra were compared to one another to observe the general, common spectral characteristics (e.g., slope, band shape, and band depth), and the best segments of the spectra representing the mineral reflectance were scaled and spliced together to form a "Frankenspectrum" for each mineral that best represents the full wavelength range of far-ultraviolet, visible, near-infrared, and middle-infrared wavelengths. These scaled and spliced Frankenspectra, as well as the entire set of individual "original" reflectance spectra from each laboratory, are available in the Planetary Data System Geosciences Node.

Unified Astronomy Thesaurus concepts: Infrared spectroscopy (2285); Ultraviolet spectroscopy (2284); Spectroscopy (1558); Vibrational spectroscopy (2249)

1. Introduction

The surfaces of many planetary bodies (including the Moon, Earth, Mars, large asteroids, and others) contain a substantial amount of fine-particulate dust (e.g., Christensen 1986; McKay et al. 1991; Ruff & Christensen 2002; Masiero et al. 2009), which we define here as sub-10 μm particulate material. To interpret remote-sensing data sets of planets, moons, and asteroids more accurately, the finest-particle geologic materials must be studied in addition to the rocks and coarse regolith because this finest fraction can dominate the optical properties of bulk soils (e.g., Pieters et al. 1993). The character of the dust also must be understood to facilitate human exploration of the Moon and perhaps Mars, the Martian moons, or asteroids. Apollo astronauts found lunar dust to be problematic. In an Apollo 17 mission debrief, astronaut Gene Cernan stated that "dust is probably one of our greatest inhibitors to nominal operation on the Moon. I think we can overcome other physiological or physical or mechanical problems except dust."

Reflectance data are useful for the study of planetary bodies via telescopes, orbital missions, or surficial rovers, and there exist numerous spectral libraries of mineral reflectance data, such as the ASTER Spectral Library (Baldridge et al. 2009), USGS Spectral Library (Kokaly et al. 2017), RRUFF Project (University of Arizona), RELAB Spectral Database (Brown University), and the Johns Hopkins University Spectral Library. Such spectral libraries, and others, are often focused on discrete spectral ranges of coarse particulates (typically >250 μm) or bulk "fine" fractions (e.g., <45 μm) for ease of data acquisition; however, it is well known that the character of spectral data is influenced by the physical state of the samples studied, including particle size (e.g., Lyon 1964; Vincent & Hunt 1968; Aronson & Emslie 1973; Salisbury & Eastes 1985; Mustard & Hays 1997; Lane & Christensen 1998). The main objective of this study is to focus on the development of a suite of reflectance spectra of 27 fine-particulate (<10 μm as defined but actually dominated by 1–2 μm particles, Section 2.2) terrestrial minerals to aid future interpretations of dusty planetary surfaces.

Another advantage of this study, in addition to our fine-particle samples, is that our data were acquired at four different laboratories using different spectrometers and setups (e.g., variations in hardware, illumination type and strength, aperture size, calibration standards, sample cups, etc.) using distributed splits from the same bulk sample of each mineral. By comparing spectra of our samples measured at disparate laboratories, we identified a few calibration/data acquisition issues that were then remedied, thus improving all future data acquired in those labs. Multiple-laboratory spectral comparisons are useful not only for identifying data collection issues but also for increasing confidence in determining both accurate spectral shapes and overall representative reflectance values by considering the reflectance data of each sample as an ensemble. This strategy is particularly helpful for the historically less-studied ultraviolet (UV) region of the spectrum, for which published spectra of geologic materials are sparse.

Additionally, this work provides reflectance spectra of minerals across a very wide spectral range. Traditionally, researchers focus on one segment of this broad wavelength range, and a sample might not be measured in a neighboring spectral range. This project unifies what might typically be several spectral studies into one broad-spectral-range study, which is scientifically impactful because spectral characteristics arise from different physics (e.g., charge transfer, molecular vibrations, etc.), and consideration of the full spectrum provides significant information about each shared sample. The resultant far-UV through mid-infrared (MIR) reflectance spectra of common minerals will be invaluable for interpreting data from the surfaces of dusty planetary bodies.

2. Characterizing the Samples

2.1. Sample Names and Chemistries

The 27 mineral samples used in this study are shown in Figure 1 and Table 1 and were chosen because they are common on Earth, the Moon, or Mars, and presumably other solar system bodies. The compositions of standards purchased from the Clay Minerals Society (CMS) and the Centre de Recherches Pétrographiques et Géochimiques (CRPG) are well established; others mineral samples were previously studied (e.g., Byrne et al. 2015) or were synthesized with controlled chemistries, and the compositions of the remaining samples were determined by electron microprobe, as noted in Table 1.

2.2. Particle Size Analyses

To obtain fine particulates, each sample was placed into a Retsch Mixer Mill 400 benchtop mill for 1–5 minutes until the sound changed to indicate that fine powder had been produced. The resultant samples were all sub-10 μm particle diameter (our maximum desired size) as verified using a particle size analyzer (Malvern Mastersizer 3000), as follows. A small amount of each sample was run in a distilled water suspension on the Hydro LV (large volume). The particle size profiles for our mineral samples are shown in Table 2.

Although the goal was to study sub-10 μm particles, this sample preparation produced samples whose true nature was skewed to finer sizes, averaging a particle diameter closer to 1–2 μm (Figure 2).

3. Laboratories Acquiring Optical Spectroscopy Data

Four different labs were used to acquire the fine-particulate reflectance spectra including the University of Colorado Laboratory for Atmospheric and Space Physics (CU LASP; Boulder, CO), the Planetary Science Institute (PSI; Tucson, AZ), the University of Winnipeg's (UW; Manitoba, Canada) Centre for Terrestrial and Planetary Exploration Planetary Spectrophotometer Facility, and the Planetary Emissivity Laboratory (which performs reflectance as well as emissivity measurements) at the German Aerospace Center (Deutsches Zentrum für Luft- und Raumfahrt, DLR) in Berlin, Germany. Mineral samples were measured in reflectance at these labs and the specifications of the instruments are as follows.

3.1. CU UV

Reflectance measurements acquired at LASP were conducted using a customized f/4.5 modified Seya-Namioka scanning-grating monochromator (McPherson, Inc. model 234/302)

Vacuum UltraViolet Analytical Spectrophotometer. Data for this work were acquired over the spectral range of far-UV into the visible (VIS) range (usable from 0.12 to 0.6 μm; 120 to 600 nm) with a spectral sampling interval of 2 nm (4 nm spectral resolution). The incidence, emission, and phase angles were 30°, 0°, and 30°, respectively. The sample cup, made of a vacuum-compatible plastic, was 1.9 cm in diameter and 0.6 cm deep. Each sample was poured into a sample cup and scraped flat with a stainless steel chemist's spatula so the powder was even with the top surface of the sample cup but not compressed. Each complete CU spectrum is a composite of four spectra obtained within the narrower, overlapping ranges of 120–240 nm, 210–320 nm, 290–400 nm, and 360–600 nm, under vacuum conditions. This strategy is required due to large variations in lamp brightness and instrument sensitivity, necessitating optimization of the photomultiplier tube (PMT) high voltage (HV) in each range. The lamp was either a 30 W deuterium (D2) lamp or a 100 W quartz-tungsten-halogen (QTH) lamp, selectable with an imaging mirror mounted to a manual rotation stage. A choice of two gratings with different ruling densities, spectral coverage, and dispersion was selected. To suppress multiple grating orders, one of several long-pass spectral filters was placed in the optical path using a manually actuated wheel located just before the monochromator entrance slit. A pair of mirrors located just after the exit slit collimated the quasimonochromatic beam. The detector was a tilted scintillator (sodium salicylate) plate coupled to a reflective light pipe, feeding a PMT operated in analog mode that was located outside the chamber and read out using a picoammeter. It should be noted that the detector gain (controlled by PMT HV) is held fixed for each wavelength range, and so the resulting reflectance is independent of this parameter. Instrument configuration for each of the spectral ranges is listed in Table 3.

Acquisition of each contributing spectrum was automated and used a fixed configuration (source, filter wheel position, grating, detector angle, and PMT HV). For each specified wavelength range, five individual measurements were acquired: (1) detector background, (2) source, (3) sample, (4) source, and (5) detector background. A background measurement typically consisted of 100 detector readouts with the source blocked using the opaque element in the filter wheel at a fixed grating position. The source was observed by positioning the sample stage to an unpopulated position, allowing the incident beam to pass through and onto the detector head that had been rotated into position. A thin, metal shield surrounds the detector head, with an aperture that is slightly larger than the collimated beam, ensuring that all incident light on the sample is collected. The sample was moved into the beam, and the detector was rotated to be normal to the sample (emission angle is 0°) for the sample measurement. Repeat measurements of the source and background were obtained to characterize any variation. The typical maximum deviation between the first and second source measurements was found to be <2%, while changes in the mean detector background signal were typically less than the random uncertainty.

This routine allows for the direct measurement of absolute sample reflectance without the need for a reference surface of idealized properties. The reflectance is calculated by

$$\Omega \frac{N_S - N_B}{N_L - N_B}, \tag{1}$$

where Ω is the empirically determined solid angle of the detector, N_S is the measured signal (photocurrent) spectrum of
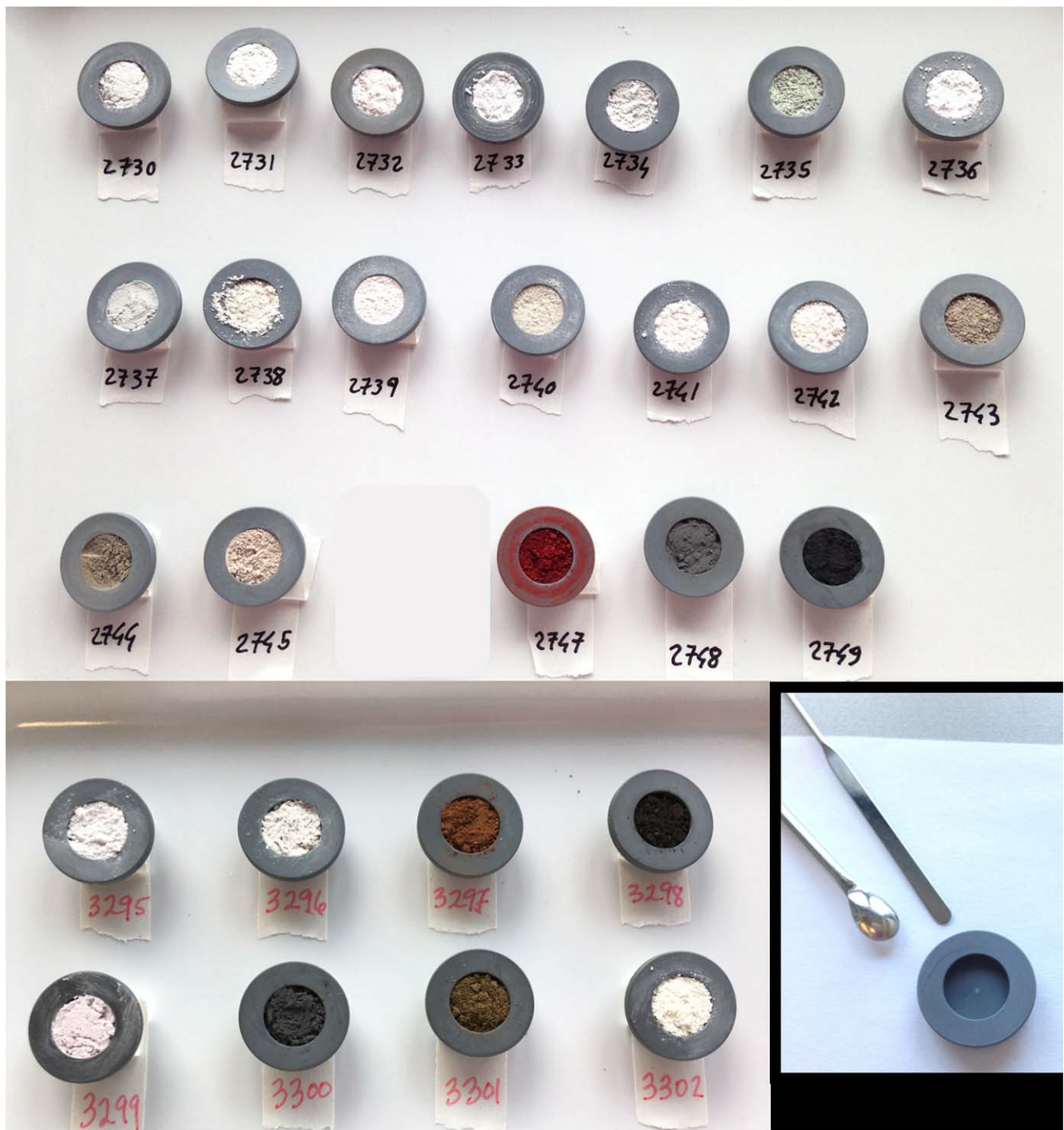
Figure 1. Photographs of our samples in the cups used for reflectance measurements at the German Aerospace Center (Deutsches Zentrum für Luft- und Raumfahrt, DLR) in Berlin, Germany. The circular well for each sample is ∼10 mm across and 2 mm deep. Samples are as follows (left to right): top row—forsterite, Globe; forsterite, SC; bytownite; labradorite, Chihuahua; diopside; augite; albite; second row—anorthite; palygorskite; hectorite; Na-montmorillonite; Ca-montmorillonite; kaolinite; serpentine UB-N; third row—phlogopite; zinnwaldite; hematite; Fe-metal; graphite; fourth row—labradorite, ARSAA; enstatite; ilmenite; pyrite; fifth row— oldhamite; spinel; nontronite; serpentine, SMS-16.

the sample, N_B is the average detector background, and N_L is the measured signal of the source lamp.

3.2. PSI UV and Visible/Near-infrared

Reflectance measurements at the PSI spectroscopy lab were taken with two spectrometers with usable wavelength ranges of 0.22–0.8 μm (at 0.376 nm spectral sampling) and 0.35–2.5 μm

(at 1 nm spectral sampling as resampled internally and output by the instrument) at ambient room temperature and pressure (25°C, 95 kPa atmospheric pressure, 20%–30% relative humidity). Both measurements were acquired using biconical reflectance. Samples were poured into a machined aluminum alloy sample cup and scraped flat with a stainless steel chemist's spatula so the powders were even with the sample cup walls but not compressed. The 0.2–0.88 μm wavelength

Table 1
Terrestrial Mineral Samples

Mineral Name	Chemistry
Albite (AL-I)[a]	$Na_{0.89}Ca_{0.02}K_{0.01}P_{0.01}Sr_{0.01}H_{0.08}Al_{0.95}Si_{3.02}O_8$
Anorthite (AN-G)[a]	$Ca_{0.79}Na_{0.15}Mg_{0.12}Fe^{2+}_{0.09}Ti_{0.01}K_{0.01}H_{0.19}\,(Al_{1.63}Fe^{3+}_{0.03})Si_{2.15}O_8$
Augite (Harcourt)[b]	$Ca_{0.94}Mg_{0.68}Na_{0.03}Mn_{0.01}Al_{0.02}Fe_{0.31}Si_{2.01}O_6$
Bytownite (Crystal Bay)[b]	$Ca_{0.65}Na_{0.33}Mg_{0.01}K_{0.01}Al_{1.62}Fe_{0.02}Si_{2.35}O_8$
Diopside (Herschel)[b]	$Ca_{0.96}Mg_{0.89}Na_{0.03}Al_{0.12}Fe_{0.06}Si_{1.95}O_6$
Enstatite (Zen-1)[c]	$Mg_{1.81}Ca_{0.01}\,Mn_{0.01}Al_{0.01}Fe_{0.18}Si_{1.99}O_6$
Fe-metal (AA-70)[d]	Fe (99.5%)
Forsterite (Globe)[b]	$Mg_{1.82}Fe_{0.18}Ni_{0.01}SiO_4$
Forsterite (San Carlos)[b]	$Mg_{1.81}Fe_{0.19}Ni_{0.01}SiO_4$
Graphite (AA-30)[d]	C (99%)
Hectorite (SHCa-1)[e]	$Ca_{4.29}\,Mg_{3.90}Na_{0.42}\,Al_{0.14}Fe^{2+}_{0.04}K_{0.03}P_{0.01}Li_{1.50}F_{1.41}\,Si_{5.94}H_4O_{22}$
Hematite (SA-500G)[d]	Fe_2O_3 (>96%)
Ilmenite (AA-30)[d]	$FeTiO_3$ (99.8%)
Kaolinite (KGa-1b)[e]	$Al_{4.07}K_{0.01}P_{0.01}Fe^{2+}_{0.01}Ti_{0.09}Fe^{3+}_{0.01}\,Si_{3.84}H_8O_{14}$
Labradorite (ARSAA)[c]	$(Ca_{0.57}Na_{0.44}Fe_{0.02}K_{0.01})Al1_{.62}Si_{2.38}O_8$
Labradorite (Chihuahua)[b]	$(Ca_{0.59}Na_{0.39}Fe_{0.01}Mg_{0.01}K_{0.02})Al_{1.60}Si_{2.39}O_8$
Ca-montmorillonite (STx-1b)[e]	$(Ca_{0.19}Na_{0.06}K_{0.01}P_{0.01}F_{0.03})[Al_{2.15}Ti_{0.02}Fe^{3+}_{0.06}Fe^{2+}_{0.10}Mg_{0.63}]\,Si7_{.98}O_{20}(OH_{1.90})_4$
Na-montmorillonite (SWy-3)[e]	$(Ca_{0.23}Na_{0.38}K_{0.09}F_{0.04}\,Fe^{2+}_{0.03}P_{0.03})[Al_{2.94}Ti_{0.01}Fe^{3+}_{0.32}Mg_{0.58}]Si_{7.99}O_{18}(OH)_4$
Nontronite (NAu-2)[e]	$Al_{0.53}Fe^{3+}_{3.74}Mg_{0.07}Ca_{0.38}Na_{0.03}Si_{7.57}H_4O_{22}$
Oldhamite (AA-14)[d]	CaS (99.9%)
Palygorskite (PFl-1)[e]	$Al_{1.63}Ti_{0.05}Fe^{2+}_{0.04}Fe^{3+}_{0.30}Mg_{2.03}Ca_{0.28}Na_{0.01}Mn_{0.01}K_{0.14}P_{0.45}F_{0.23}\,Si_{8.11}H_{4.00}O_{22}$
Phlogopite (Mica-Mg)[a]	$Al_{0.05}Ti_{0.22}Fe^{2+}_{1.03}Fe^{3+}_{0.27}Mg_{5.55}Mn_{0.04}Ca_{0.02}Na_{0.04}K_{2.33}P_{0.01}\,Si_{6.99}H_{2.54}O_{24}$
Pyrite (SA-25G)[d]	FeS_2 (99.8%)
Serpentine (SMS-16)[c]	$Mg_{2.83}Fe^{3+}_{0.02}Si_{2.07}H_{4.01}O_9$
Serpentine (UB-N)[a,f]	$Mg_{2.59}Al_{0.17}Fe^{2+}_{0.11}Fe^{3+}_{0.20}Mn_{0.01}Ca_{0.06}Na_{0.01}P_{0.01}Si_{1.94}H_{3.56}O_9$
Spinel (ARSAA)[c]	$Al_{1.98}Mg_{0.99}Ba_{0.03}Fe^{2+}_{0.01}O_4$
Zinnwaldite (ZW-C)[a]	$Ca_{0.06}Na_{0.10}K_{1.48}Al_{3.26}Fe^{3+}_{0.15}Fe^{2+}_{0.92}Mg_{0.04}Mn_{0.12}P_{0.02}Ti_{0.01}\,Si_{8.10}O_{24}H_{1.46}$

Notes.
[a] CRPG standard.
[b] Byrne et al. (2015).
[c] Our electron microprobe analysis.
[d] Synthesized (AA from Alfa Aesar; SA from Sigma-Aldrich).
[e] CMS standard.
[f] UB-N is from the "2015 lot" and has a lizardite structure (Gayk & Kleinschrodt 2000; Hallatt et al. 2021).

range was taken with an Ocean Optics UV-Flame spectrometer, using a fiber optic cable, with a spectral resolution of 1.4 nm FWHM at an incidence angle of 0° and 30° emission angle; phase angle was 30°. Illumination was provided with a combined D2 arc lamp (0.2–0.5 μm) and quartz halogen light source (0.4–0.88 μm), with light transmitted to the sample via a fiber optic cable. The 0.35–2.5 μm range was acquired with an Analytical Spectral Devices FieldSpec 3 with a 25° field-of-view fiber optic cable bundle held ∼3 cm from the sample, resulting in a spot size ∼2.6 cm across. Spectral resolution was 3 nm FWHM in the 0.35–1.0 μm range and 10 nm FWHM resolution from 1.0 to 2.5 μm, and the geometry of the measurements was the same as for the Ocean Optics measurements. Illumination was provided by a bare quartz halogen full spectrum bulb 40 cm above the sample. Measurements were taken relative to a flat Spectralon® standard that was positioned at the same height as the sample. Spectralon® artifacts, particularly a common inverted 2.15 μm absorption feature, were then corrected for during post-processing by multiplying the sample spectrum by a calibrated Spectralon®

Table 2
Particle Size Distribution of Mineral Samples

Mineral Name	Dn (90)[a] (μm)	Dn (50)[a] (μm)	Dn (10)[a] (μm)
Albite (AL-I)	1.562	0.8355	0.613
Anorthite (AN-G)	1.503333	0.796	0.594
Augite (Harcourt)	1.341	0.7576	0.577
Bytownite (Crystal Bay)	1.52	0.8174	0.606
Diopside (Herschel)	1.4264	0.77728	0.58936
Enstatite (Zen-1)	1.35	0.7526	0.5739
Fe-metal (AA-70)	5.023	2.669	1.682
Forsterite (Globe)	1.46	0.8018	0.602
Forsterite (San Carlos)	1.47	0.799	0.6008
Graphite (AA-30)	3.946	1.24	0.652
Hectorite (SHCa-1)	1.6324	0.78664	0.59192
Hematite (SA-500G)	0.02435	0.01475	0.011
Ilmenite (AA-30)	1.43	0.6885	0.4701
Kaolinite (KGa-1b)	1.466	0.7327	0.53815
Labradorite (ARSAA)	1.812	0.868533	0.655467
Labradorite (Chihuahua)	1.64	0.861	0.651
Ca-montmorillonite (STx-1b)	1.893	0.86412	0.61592
Na-montmorillonite (SWy-3)	1.668	0.7944	0.5736
Nontronite (NAu-2)	3.1045	1.17745	0.8012
Oldhamite (AA-14)	0.8448	0.4839	0.3419
Palygorskite (PFI-1)	4.72	2.077	1.294
Phlogopite (Mica-Mg)	2.442	1.043	0.7403
Pyrite (SA-25G)	0.024453	0.01478	0.011
Serpentine (SMS-16)	1.78	0.843	0.6129
Serpentine (UB-N)	1.2	0.71896	0.537
Spinel (ARSAA)	1.377333	0.7338	0.543067
Zinnwaldite (ZW-C)	1.56	0.8001	0.601

Note.
[a] Dn 50 is the size in microns at which 50% of the sample is smaller and 50% of the sample is larger, and n is the number distribution. Accordingly, Dn 90 or Dn 10 is the size of the particle below which 90% or 10% of the sample lies, respectively.

reflectance spectrum. This process is described in more detail in Clark et al. (1990) and Kokaly et al. (2017).

3.3. UW Visible/Near-infrared

Reflectance spectra from 350 to 2500 nm (0.35 to 2.5 μm) were measured at ambient temperature and pressure relative to a calibrated Spectralon® 99% diffuse reflectance standard with an Analytical Spectral Devices (ASD) LabSpec4 Hi-Res spectrometer at an incidence angle of 30°and emission angle of 0°. These spectra were corrected for the absorption features
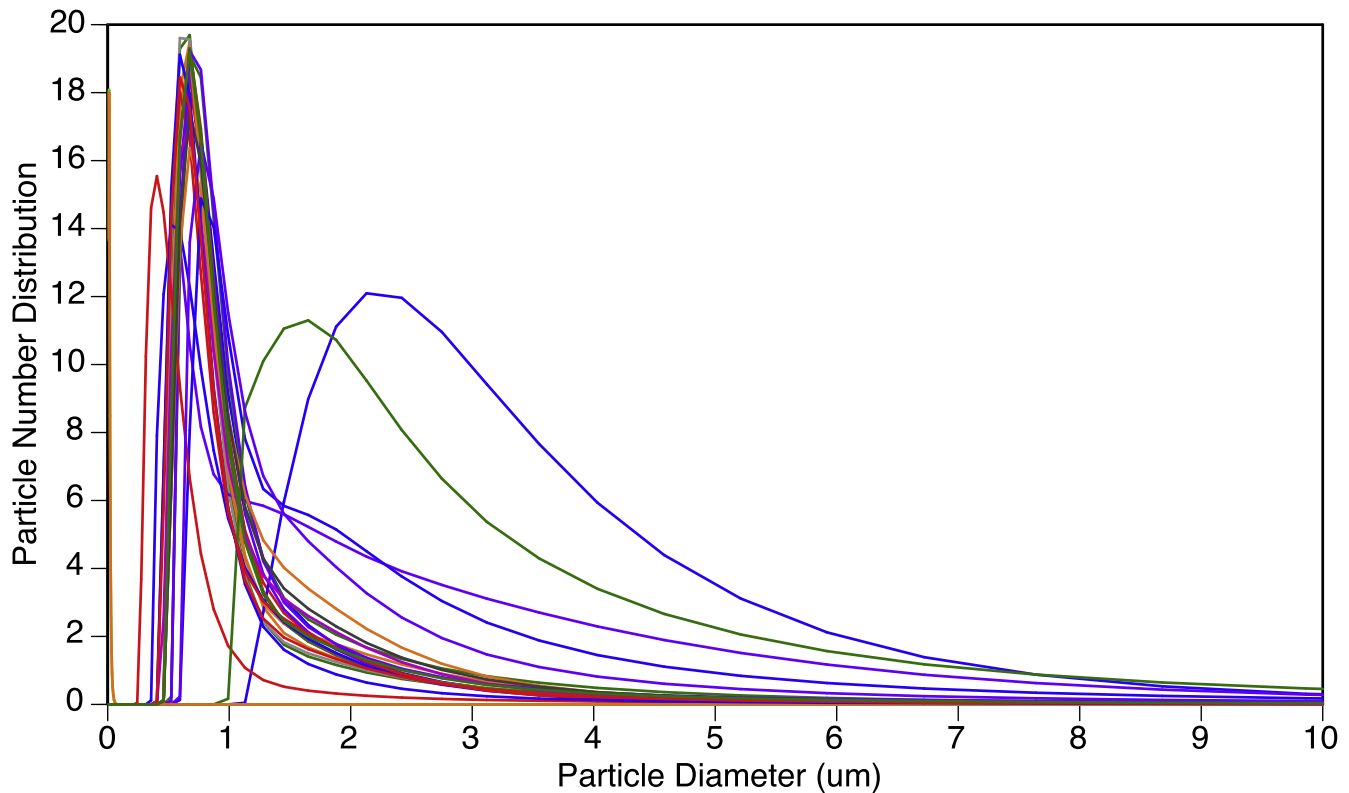
of Spectralon® as measured by Labsphere according to the ASTM-E1331 standard (formerly known as the American Society for Testing and Materials). For measurement, the mineral powders were poured into an aluminum sample cup by first gently pouring, then tapping the cup several times, and finally scraping the excess off with a glass slide held away from the sample at 45°. The sample cups were variably sized but were all deep enough to ensure no contribution to the measurements. All sample cups were painted black so that their reflectance was measured to be lower than 3% over the wavelength range measured. The field of view was varied for the measurements but was confined to the powder and overfilled by the light source. An in-house quartz-tungsten halogen light source was used to provide incident light that was collimated to <1.5° divergence with a cold color temperature that provides sufficient signal-to-noise ratio over the three sensors of the ASD instrument, with flux sufficiently low to not induce observable emittance on very dark samples in the wavelength range under study.

The reflected light is collected by a 2 m long, 1.85 mm wide core fiber optic bundle comprised of 44 separate silica fibers (numerical aperture = 0.22) with internal diameters of 200 μm. The light collected from the fibers is injected into an internal light scrambler, followed by injection into three separate bundles, one comprised of 19 100 μm diameter silica fibers that feeds the Si-diode array (350–1000 nm wavelength range) and two bundles comprised of nine 200 μm diameter silica fibers that feed the two InGaAs systems (1000–1850 nm and 1850–2500 nm wavelength range). The LabSpec4 Hi-Res (high resolution) has a spectral sampling interval of 1.4 nm for the Si-diode array and 2.2 nm for the two InGaAs systems. The spectral resolution for the Si-diode array is 3 nm centered at 700 nm and 6 nm centered at both 1400 nm and 2100 nm for the InGaAs systems. The resulting spectra were resampled internally by the instrument to output data at 1 nm intervals via a proprietary cubic spline fit to the sampled spectra. Five hundred scans of reflectance spectra were collected for each sample, and 500 scans of dark current were subtracted from sample and standard reflectance spectra.

3.4. DLR UV, Visible, and MIR

Reflectance measurements were acquired in the Planetary Spectroscopy Laboratory in Berlin. The lab is outfitted with two Bruker Vertex80V FTIR spectrometers, each with a Bruker A513 unit that enabled bidirectional reflectance measurements. The instruments are under vacuum at a pressure of 0.7 mbar, and all measurements were made at ambient temperature. The incidence, emission, and phase angles were 30°, 0°, and 30°, respectively. The measurements were acquired over the total spectral range of 0.25–20 μm.

The UV data ranged from 0.25 to 0.45 μm. Initially some data (19 samples) were measured at 4 cm^{-1} sampling, but the spectra of the remaining eight samples were retrieved at 16 cm^{-1} sampling, which was adequate for the UV range. The spectrometer's incident beam was stepped down to a 3 mm aperture before the mirrors, creating a spot size on the sample no larger than ∼5 mm, which was well inside the 10 mm cross section of the sample in the cup. The spectrometer housed a gallium phosphide (GaP) detector and a CaF$_2$ beamsplitter. The samples were illuminated by a D2 lamp (that produced much better results than when a tungsten lamp was used initially).

Figure 2. Particle size distributions of the mineral samples as acquired using a Malvern Mastersizer 3000 with a Hydro LV attachment. The *y*-axis shows the number distribution, i.e., for all the particles measured of a single sample; they sum to 100%. All of the samples are much finer than the target of being <10 μm diameter and are representative of "dust" sizes that are on solar system bodies. The two larger-skewed samples are palygorskite (green) and Fe-metal (blue).

The sample spectra (an average of 1000 scans) were calibrated against a polytetrafluoroethylene standard.

The visible (VIS) data ranged from 0.4 to 1.1 μm and were acquired at 1 cm^{-1} sampling. The mineral samples were measured with a spectrometer, equipped with a CaF$_2$ beamsplitter and a Si-diode detector, using a 2 mm aperture with samples illuminated by an external, high-power (24V), water-cooled tungsten lamp. An initial Spectralon® powder target material was measured as a calibration step. This calibration target material was held in a small Teflon^{TM} cup that was identical to the cups used for holding the powdered mineral samples. Each cup has a short cylindrical trough for the sample that is 10 mm across and 2 mm deep. The output reflectance spectrum was an average of 500 scans.

The MIR (which actually extends shortward into the near-infrared, NIR) covers the spectral range from 1.0 to 20 μm. The samples were measured, through a 0.25 mm aperture, using a spectrometer housing a mercury-cadmium-telluride detector and a KBr beamsplitter. The samples were illuminated with an external, water-cooled Globar®. The output "MIR" reflectance spectrum was an average of 500 scans (at 2 cm^{-1} spectral sampling) calibrated to an Infragold® diffuse reflectance target.
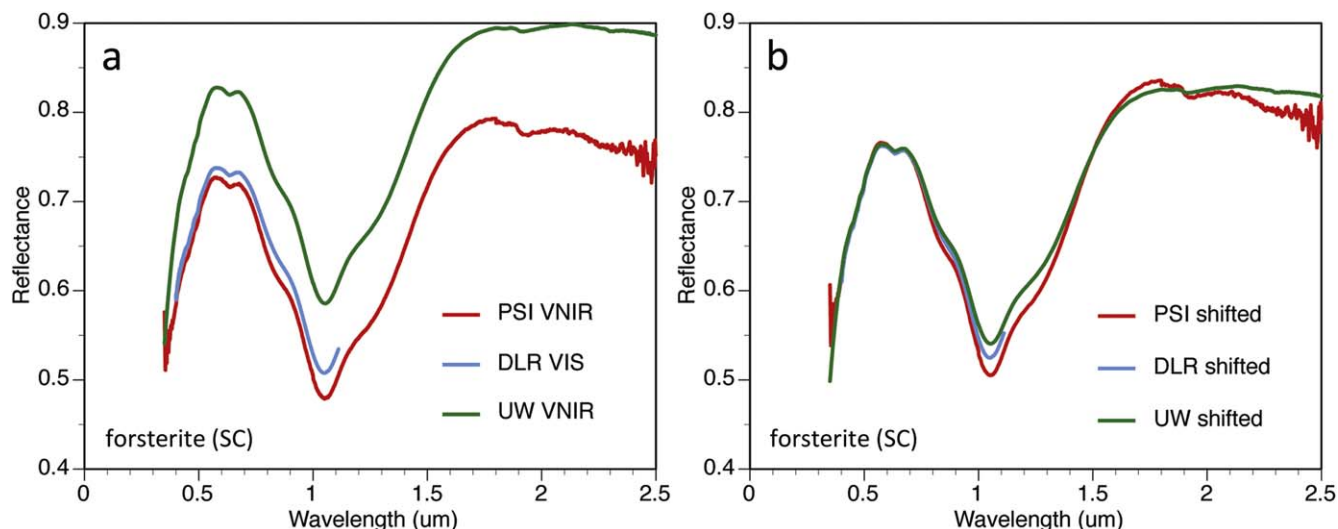
Figure 3. Establishing the baseline spectrum in the visible range on which each Frankenspectrum is built, using fine-particulate forsterite (San Carlos) as an example. (a) Original PSI VNIR, DLR VIS, and UW VNIR data. (b) Spectra multiplicatively shifted to the average reflectance value at 0.7 μm. For the forsterite (San Carlos) Frankenspectrum, the shifted UW VNIR data were used for the baseline spectrum segment (Table 4).

Table 3
CU LASP Instrument Configuration for Each Spectral Range in a "UV" Composite Spectrum

Lamp	Filter (nm)	Entrance Slit Width (mm)	Exit Slit Width (mm)	Grating (gr/mm)	Bandpass (nm)	Wave Start (nm)	Wave Stop (nm)	Wave Step (nm)	Peak Wavelength (nm)	HV for Peak Signal
D2	...	1	1	1200	4	90	250	2	160	481
D2	210	1	1	1200	4	150	450	2	230	700
QTH	...	0.5	0.5	600	4	150	400	2	400	431
QTH	350	0.5	0.5	600	4	300	600	2	600	320

4. Making "Frankenspectra"

It is rare that multiple spectra of a single sample, measured at different laboratories, would plot identically, even if they were prepared into sample cups as similarly as possible. Typically, there are offsets, varied slopes, brightness differences (from differences in sample surface roughness or hardware), spikes (from illumination sources or atmospheric components, etc.), and other variations that make the spectra all slightly different from each other. But when developing a spectral library, it is ideal to minimize these differences and establish an accurate end-member spectrum that is most representative of the sample. The goal of this project is to create one reference far-UV-through-MIR reflectance "Frankenspectrum" for each sample that is considered to be the best representation of the reflectance properties of the sample across the spectral range of 0.12–20 μm. We give our scaled and spliced spectra the nickname "Frankenspectra" because, like Dr. Frankenstein who pieced his creature together from various sources (Shelley 1818), we are making one continuous spectrum built by stitching together the best segments of spectral data from different labs. The procedure developed for constructing our Frankenspectra is as follows.

4.1. Establishing the Baseline for the Frankenspectra

The initial, critical step for making the Frankenspectra was to establish a baseline for the spectrum in the visible range of the available data, to which other spectral segments get attached. To do this, the PSI visible/near-infrared (VNIR), DLR VIS, and UW VNIR data were plotted together because they were the cleanest spectra that were consistent with one another in terms of spectral shape and lack of noise (Figure 3(a)). To establish the baseline segment for the Frankenspectra, these plotted spectra were assessed to identify a good single wavelength position (on the x-axis) between 0.3 and 0.8 μm where none of the spectra exhibited distinct bands and where they had similar slopes and no spectral noise, i.e., a bland location that would be the chosen point to retrieve the average reflectance value. Once that singular position was chosen (which varied for each mineral sample but was between 0.5 and 0.8 μm for the entire suite of samples), the average reflectance value (on the y-axis) at that same chosen wavelength position was determined by averaging the three spectra (Figure 3(b)). Figure 3(b) shows all the spectra shifted to the average value at the given wavelength. However, for each Frankenspectrum, only the best representative, original single-lab spectrum was multiplicatively shifted to the average reflectance value and used further as the pinned baseline segment for the entire Frankenspectrum. For all but one sample (i.e., hematite), the UW VNIR shifted spectra were chosen as the best baseline segments for the Frankenspectra (Table 4).

4.2. Extending the Baseline Frankenspectrum to Shorter and Longer Wavelengths

Each Frankenspectrum was lengthened by selecting the best other single-lab spectra covering different wavelengths (higher

Table 4
UV-VIS-VNIR-MIR Frankenspectrum Construction Parameters for Each Mineral Sample

Mineral Sample (<10 μm Powders)	Set Point for Baseline Reflectance Value (μm)	Reflectance Value at Set Point (Average of PSI VNIR, DLR VIS, UW VNIR)	Scaling Value Applied to Original Lab Data Segments and the Relevant Splice Point								
			CU UV	Splice Point (μm)	PSI UV	Splice Point (μm)	PSI VNIR[a]	Splice Point (μm)	UW VNIR[a]	Splice Point (μm)	DLR MIR
Albite AL-I	0.5	0.822666667	1.042979943	0.35					**1.00203004**	1.8	1.372 456 964
Anorthite AN-G	0.5	0.468666667	0.96961326	0.35					**0.94489247**	1.8	1.321 033 21
Augite—Harcourt	0.6	0.397	1.007518797	0.35					**0.835789474**	1.8	1.237 442 922
Bytownite CB	0.7	0.786	1.102564103	0.25	1.144869215	0.35			**0.962056304**	1.8	1.435 314 685
Diopside Herschel	0.6	0.697	1.658227848	0.26	0.951807229	0.35			**0.914698163**	1.8	1.366 609 294
Enstatite Zen-1	0.6	0.639333333	0.915766739	0.36					**0.99895833**	1.8	1.272 988 506
Fe-metal AA-70	0.5	0.108333333	1.2	0.25	1.0	0.36			**0.887978142**	1.8	1.25
Forsterite Globe	0.7	0.708333333	1.189189189	0.30	0.932258065	0.39			**0.954627134**	1.8	1.410 681 4
Forsterite San Carlos	0.7	0.750333333	0.886764706	0.39					**0.922919229**	1.8	1.410 256 41
Graphite AA-30	0.7	0.041033333	1.323529412	0.25	0.975	0.4			**0.995954693**	1.8	1.274 725 275
Hectorite SHCa-1	0.7	0.761333333	0.931623932	0.26	1.062836625	0.4			**0.95524885**	2.42	1.195 219 124
Hematite SA-500G	0.7	0.208333333	0.962962963	0.52			**1.006441224**	1.8			1.225 806 452
Ilmenite AA-30	0.7	0.262666667	1.0	0.51					**1.210445469**	1.8	1.513 888 889
Kaolinite KGa-1b	0.7	0.844	0.88299532	0.4					**0.987134503**	1.6	1.376 175 549
Labradorite ARSAA	0.7	0.697666667	0.842465753	0.37					**1.00095648**	2.4	1.352 272 727
Labradorite Chihuahua	0.7	0.808	0.884892086	0.37					**0.925544101**	1.8	1.458 928 571
Ca-montmorillonite STx-1b	0.7	0.86	0.898448519	0.4					**0.98510882**	2.25	1.388 185 654
Na-montmorillonite SWy-3	0.7	0.540333333	0.825396825	0.4					**0.996924969**	2.26	1.262 411 348
Nontronite NAu-2	0.8	0.386	0.602409639	0.46					**1.131964809**	2.34	1.100 401 606
Oldhamite AA-14	0.67	0.629333333	1.155172414	0.26	0.951612903	0.36			**0.981799272**	2.4	1.336 397 059
Palygorskite PFI-1	0.7	0.585666667	0.745059289	0.4					**0.944623656**	2.4	1.175 718 85
Phlogopite Mica-Mg	0.62	0.239666667	0.925619835	0.36					**1.024216524**	2.0	1.298 056 156
Pyrite SA-25G	0.7	0.043333333	0.6	0.39					**1.007751938**	2.0	1.421 052 632
Serpentine SMS-16	0.54	0.816333333	0.858126722	0.37					**0.985909823**	2.2	1.336 976 321
Serpentine UB-N	0.5	0.210666667	0.858126722	0.37					**0.923976608**	2.4	1.226 244 344
Spinel ARSAA	0.52	0.087333333	0.770114943	0.4					**0.919298246**	2.42	1.266 666 67
Zinnwaldite ZW-C	0.7	0.527666667	0.886227545	0.4					**0.935579196**	2.4	1.337 142 857

Note.

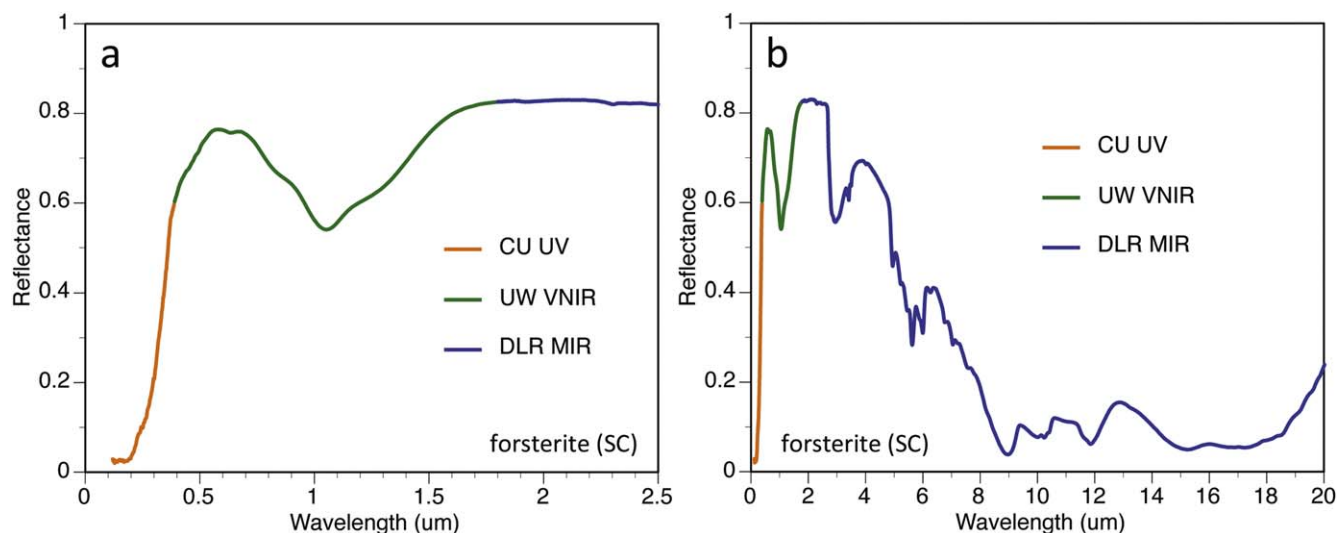[a] Baseline segment used for each Frankenspectrum is in bold.

8

Figure 4. Frankenspectrum of fine-particulate forsterite (San Carlos) showing the scaled segments of the best laboratory spectra spliced to the baseline spectrum, as an example. The single Frankenspectrum (0.12–20 μm) is shown at two scales for clarity: (a) far-UV–VNIR (0–2.5 μm) and (b) far-UV–MIR (0–20 μm).

and lower frequencies), then scaling and splicing them to the pinned baseline visible spectrum (described in Section 4.1) or to the neighboring segment as the Frankenspectrum grew in length into other spectral regions.

Not all of the spectra available were needed to make each Frankenspectrum. Based on the quality of the data, there were multiple options for which spliced spectral segments were used; they varied from mineral to mineral but included (±) CU UV, PSI UV, PSI VNIR, UW VNIR, and DLR MIR spectra. Each spectrum chosen as the representative segment of the Frankenspectrum was selected by plotting all the available spectra (as described in Section 3) and choosing the one for that segment that was best representative of all the data (e.g., matching features, matching slopes, and low noise). Once the one lab spectrum was selected for the next segment of the Frankenspectrum, it was multiplicatively scaled, then spliced onto the Frankenspectrum at a hand-selected wavelength in the spectrally blandest region that was devoid of features with no change in slope (which varied for each mineral sample).

A detailed example Frankenspectrum of forsterite (San Carlos) is shown in Figure 4. The multiplicative scaling factors, splice points, and selected spectral segments for each Frankenspectrum are listed in Table 4, and the Frankenspectra of the entire mineral suite are shown in Figure 5 (far-UV into VNIR), Figure 6 (VNIR), Figure 7 (NIR into MIR), Figure 8 (MIR), and Figure 9 (far-UV-through-MIR full spectrum).

All data were spliced by hand. The variable wavelength positions where the splices occurred and the numerical precision required to make the splices seamless at large magnification demonstrate that this process is not easily automated.

4.3. Discussion Regarding Measurement Conditions for the Frankenspectra

As presented earlier, the samples were measured at different labs under different pressure and temperature conditions as required for the best functionality of the spectrometers, which can make a difference in the character of the spectra. In our spectra, the differences were minimal, predominantly because particle size often has the largest impact on spectral shape, and we distributed splits from the same bulk sample to each lab for the measurements.

However, there do exist small overall differences among spectra for each spectral range. For the UV, the CU measurements (acquired under vacuum) covered the widest spectral range and were the least noisy but sometimes exhibited a bend/step at ~0.37 μm due to the spectral splicing done initially at CU (see Section 3.1) to generate the "original" spectrum for each sample. Generally, if the spectrum had a pronounced step, the data were not used above 0.37 μm for the Frankenspectra. Other CU UV data did not show this step, and those data were used for Frankenspectra with the splice points located at longer wavelengths.

The DLR UV data also were acquired under vacuum. Those spectra were quite noisy, and displayed a large increase in reflectance at the high-frequency end of the spectrum (shortward of 0.25 μm) due to decreased detector efficiency. In all other ways, the DLR UV data followed the general shape and slope of the CU UV and PSI UV spectra, making them useful for comparison. However, no DLR UV data were used for the Frankenspectra due to these noted issues.

Typically, the PSI UV data acquired by the Ocean Optics instrument tended to be clean from ~0.22 to ~0.43 μm but noisier from 0.43 to 0.8 μm. However, the shape and slope matched the other data sets when plotted together, so they were also useful for comparison. Although each "UV" data set had its quirks, plotting the three data sets together always revealed the proper character of the spectrum where two (or three) of the three spectra matched in shape and slope. Beyond the differences discussed, no obvious spectral differences in the UV were attributed to vacuum-versus-ambient pressure measurements.

For the VIS/VNIR data, the PSI VNIR, the DLR VIS, and the UW VNIR spectra were very similar in shape and slope. Rarely, the DLR VIS spectra (measured under vacuum) exhibited a modified ~1 μm band (a slight dip) but were otherwise similar to the other two data sets. Thus, the DLR VIS spectra were never used for a segment of any Frankenspectrum;
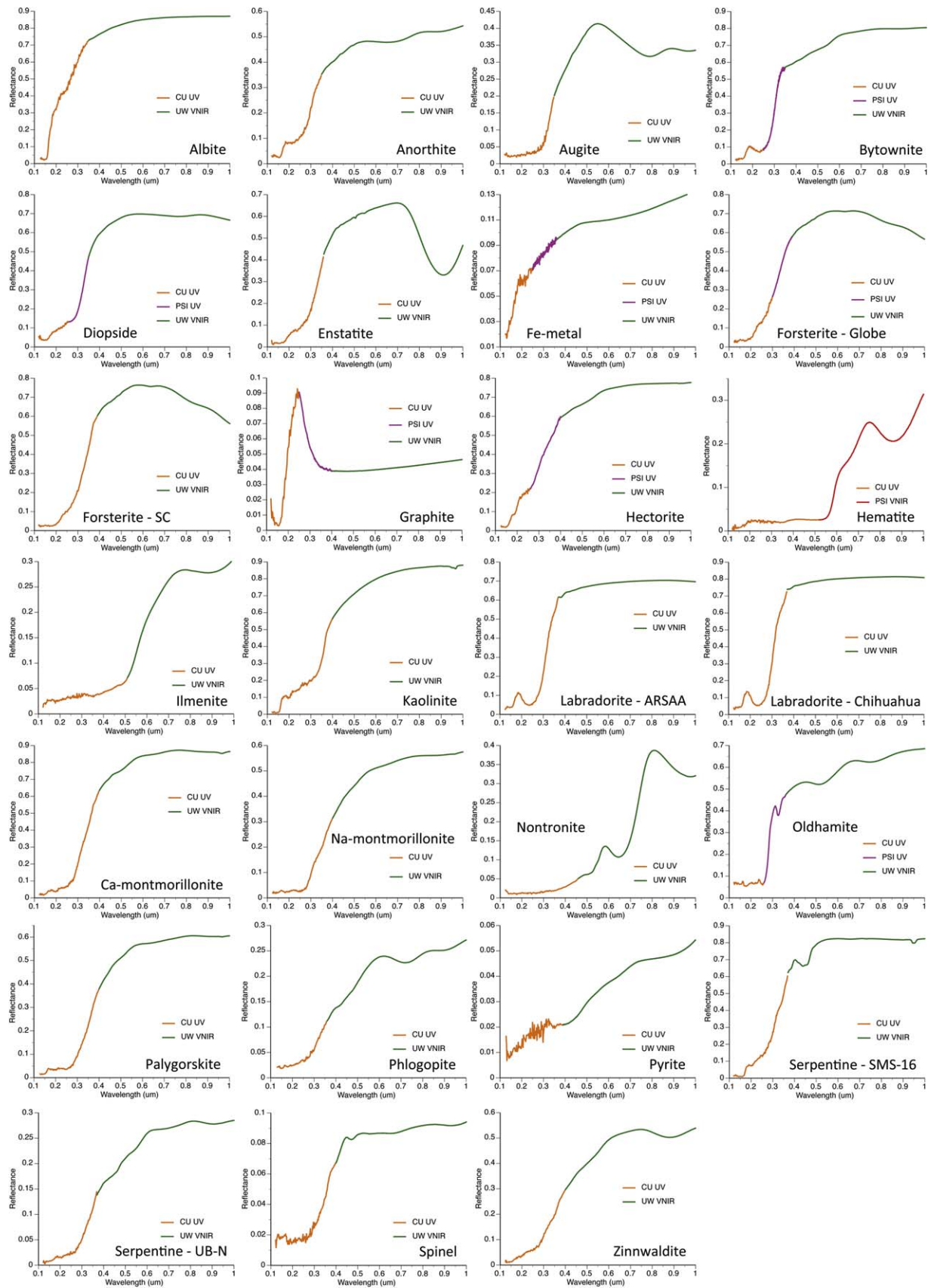
Figure 5. Frankenspectra of the 27 fine-particulate mineral samples acquired in reflectance shown over the 0.1–1.0 μm range (i.e., far-UV/VNIR).
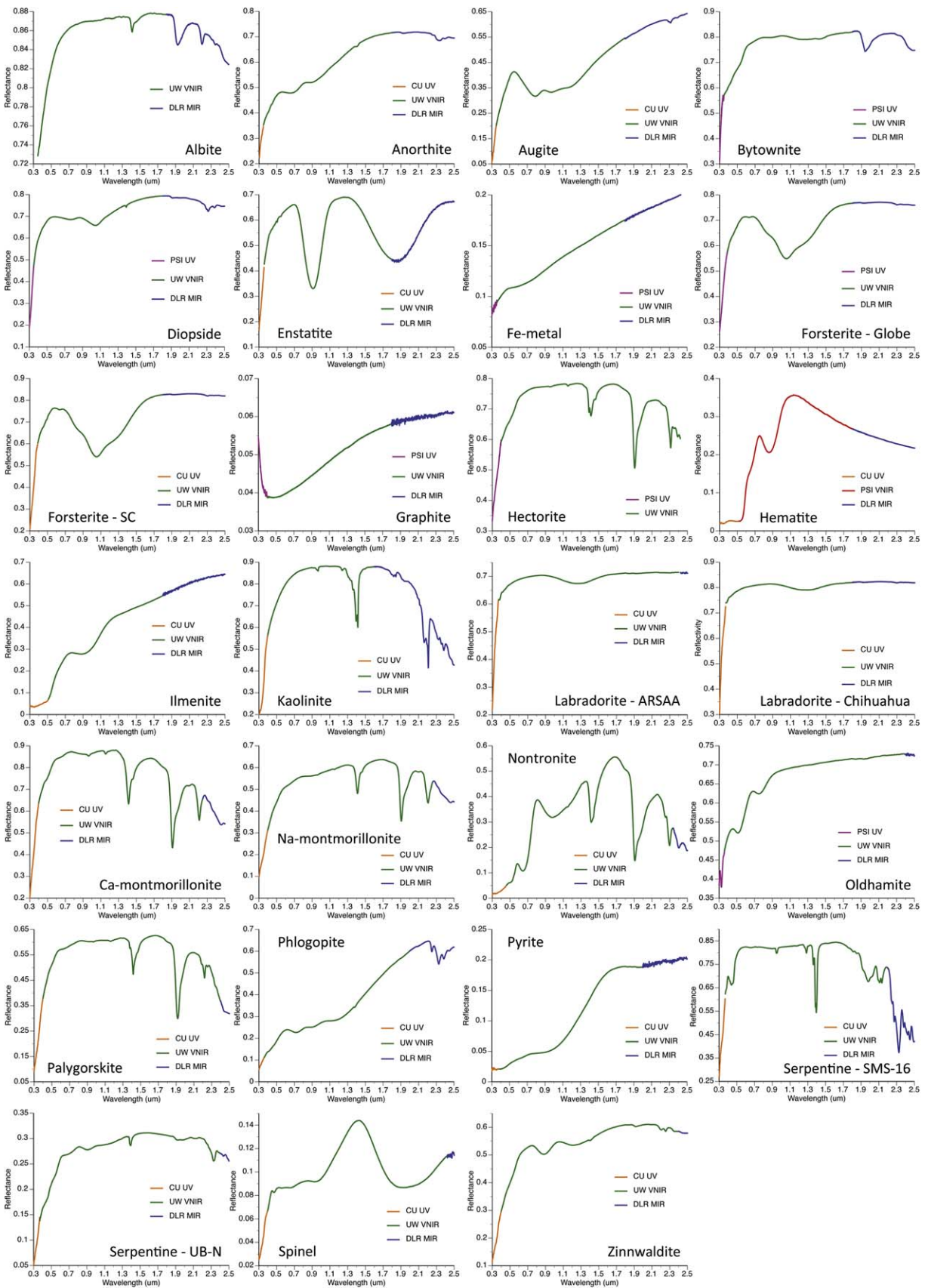
Figure 6. Frankenspectra of the 27 fine-particulate mineral samples acquired in reflectance shown over the 0.3–2.5 μm range (i.e., VNIR). The data labeled "MIR" are from a 1.0 to 20 μm single measurement at DLR.
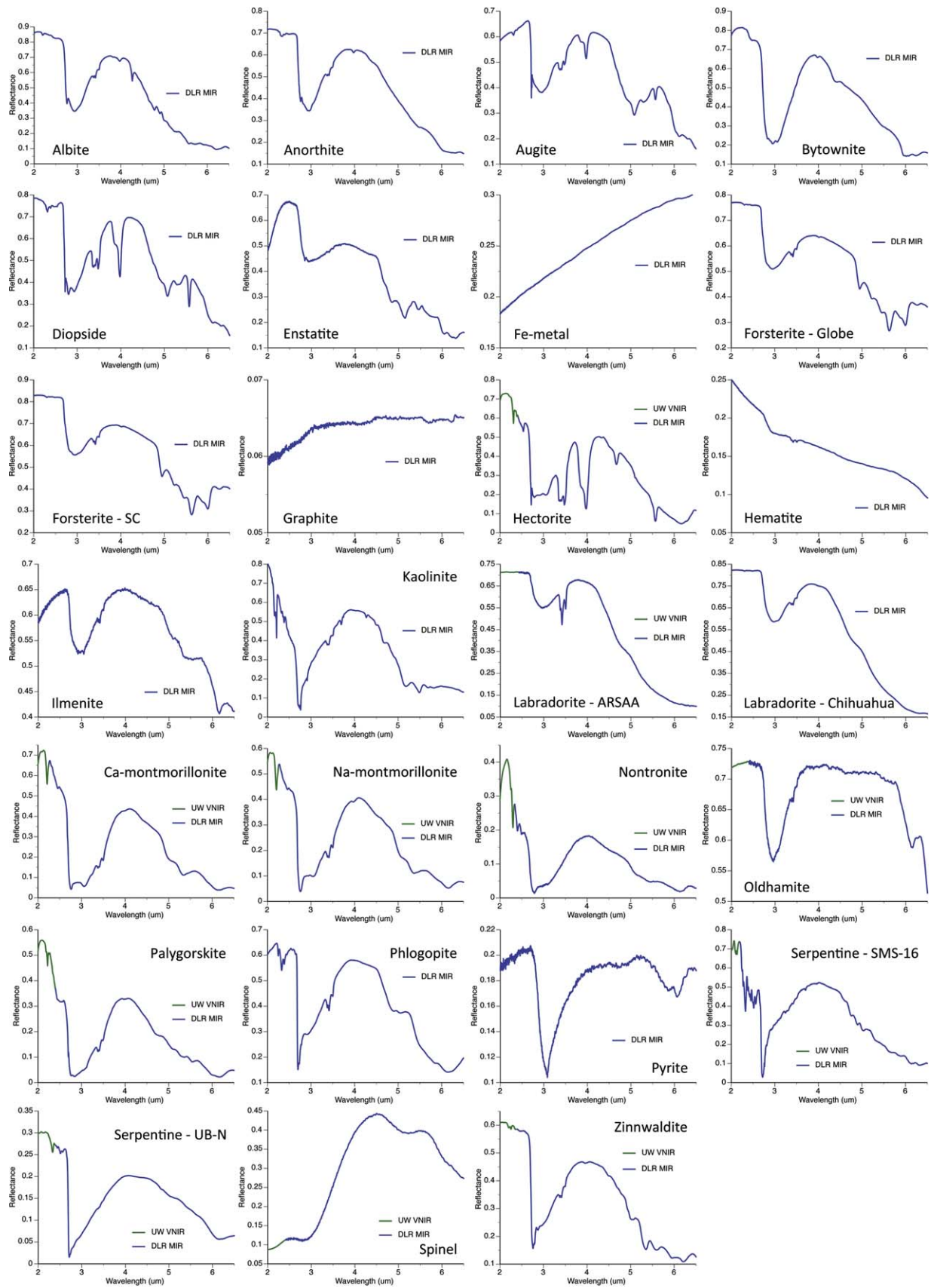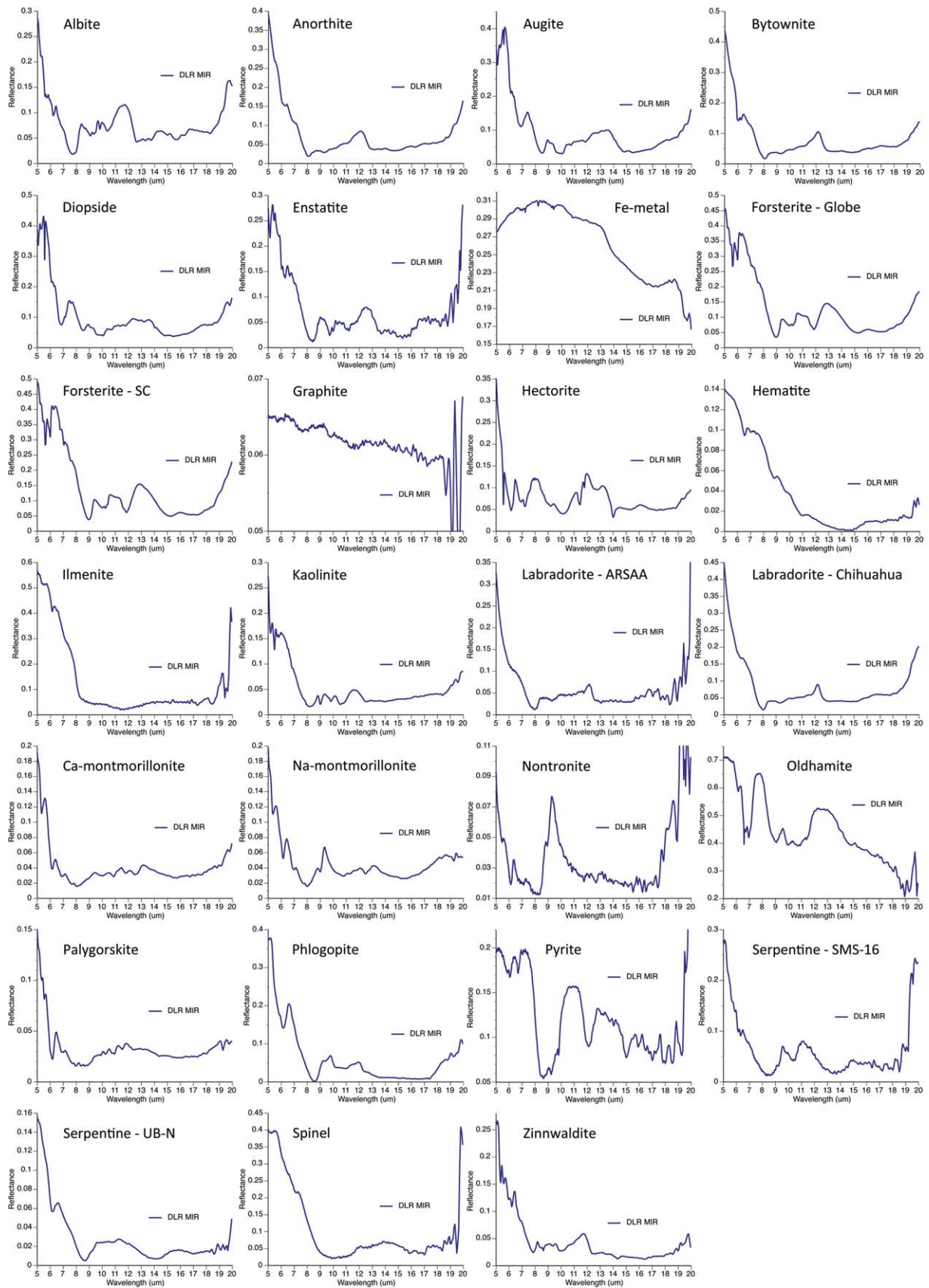
Figure 7. Frankenspectra of the 27 fine-particulate mineral samples acquired in reflectance shown over the 2.0–6.5 μm range (i.e., NIR/MIR; sometimes the ~2–3 μm range is more specifically called "short-wave" infrared and ~3–5 (or 8) μm is called "mid-wave" infrared by camera optics companies). The data labeled "MIR" are from a single 1.0 to 20 μm measurement at DLR.

Figure 8. Frankenspectra of the 27 fine-particulate mineral samples acquired in reflectance shown over the 5–20 μm range (i.e., MIR; sometimes the ~5 (or 8)–20 μm range is called "long-wave" infrared or "thermal infrared" by camera optics companies).
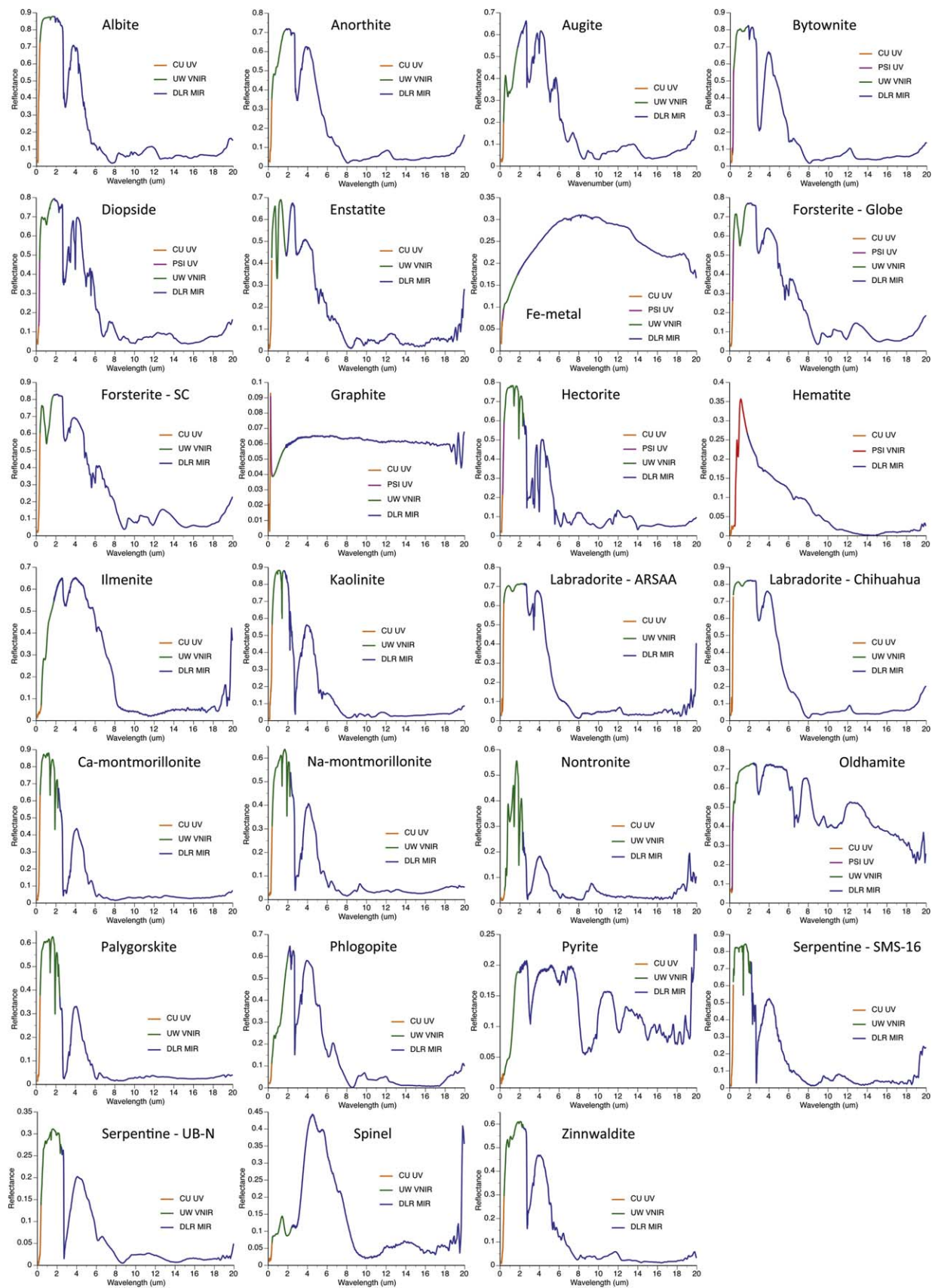
Figure 9. Frankenspectra of the 27 fine-particulate mineral samples acquired in reflectance shown over the full 0–20 μm spectral range.

however, they were used to assess, with the other two VNIR data sets, the average reflectance value for setting each Frankenspectrum baseline (see Section 4.1). The PSI and CU VNIR data were acquired under ambient environmental conditions, so there were no appreciable spectral differences due to atmospheric pressure.

Although not included in this paper, the suite of samples also was measured over the VNIR range under vacuum at DLR, but the spectra were fraught with residual Spectralon features and often displayed an upswing at the long-wavelength end of the spectra due to imperfect calibration and thus were not used for the Frankenspectra. Additional spectral differences were observed in the DLR VNIR data, as compared to the PSI VNIR and UW VNIR spectra, in terms of bands shrinking or other bands appearing due to changes in the water content of the sample. These differences were only associated with the water-bearing phyllosilicates. The largest ambient-versus-vacuum spectral difference was for hectorite, where the composite band at ~1.4 μm and the 1.9 μm band shallowed quite a bit due to dehydration of the sample. There were only slight differences in Ca-montmorillonite—the bands shrank slightly but developed a new small band at ~2.1 μm due to dehydration. In Na-montmorillonite, the bands shrank to a lesser extent than for the Ca variety, with no formation of a new band. Nontronite lost the subtle shoulder near 2.0 μm and exhibited a sharpening of the previously rounded ~1.4 μm band. Palygorskite developed a very small shoulder band at ~1.95 μm. There were no differences observed for the kaolinite, phlogopite, or either serpentine sample. But the DLR VNIR spectra otherwise generally shared the spectral character of the PSI and UW VNIR data. It is important to note that the VNIR region of the Frankenspectra is representative of minerals acquired under ambient conditions with normal hydration.

MIR measurements (that extend into the NIR range, as noted above) were acquired only at DLR, but they shared the spectral range from 1.0 to 2.5 μm with the PSI VNIR and UW VNIR (and DLR VNIR, unused for Frankenspectra) data, allowing spectral comparison over this region. The DLR MIR data were acquired under vacuum conditions, similar to the measurement conditions for the DLR VIS measurements. Thus, the MIR spectra represented slightly dehydrated samples as noted above for the DLR VNIR spectra. However, when compared to DLR MIR emissivity data (to be discussed in a separate paper) of the same samples fresh from the sample bottles and not previously in vacuum, there were no spectral differences attributable to hydration issues per se, even for hectorite. Thus, the DLR MIR data, after careful assessment, were scaled and spliced to the VNIR data and are assumed to be representative of the sample at the longer wavelengths.

5. Data Caveats

It is well known that spectral data acquired in a laboratory at ambient temperature and pressure cannot always be directly compared to planetary surface data mostly due to three factors: (1) space weathering and soil vitrification that affect both the UV region causing blue-sloped spectra (Hendrix & Vilas 2006) and the VNIR region causing characteristic sloping of spectra toward red (e.g., Adams & McCord 1971; Pieters 1986; Pieters et al. 1993) or possibly blue (e.g., Lantz et al. 2017), (2) an additional thermal component that effectively shallows or masks the reflectance bands,

depending on the temperatures involved, longward of ~2.2 μm for the Moon and near-Earth asteroids and ~3 μm for Mars (e.g., Pieters 1986; Blaney & McCord 1989), and (3) temperature gradients in MIR data associated predominantly with atmosphere-less bodies such as the Moon and asteroids that are exacerbated by fine-particle sizes (thus causing shifting of the Christiansen feature, CF, to shorter wavelengths and affecting the overall spectral contrast and character (e.g., Logan & Hunt 1970; Donaldson Hanna et al. 2012; Shirley & Glotch 2019; Bramble et al. 2021).

Laboratory studies by Hinrichs & Lucey (2002) showed that VNIR spectra of fine-particle mineral samples are modified somewhat over a wide range of temperatures, but the changes are slight and would not deter their identification. Furthermore, for fine mineral mixtures, meteorite powders, and lunar soils, such thermal effects on VNIR spectra were further reduced. This spectral behavior has implications for quantitatively interpreting VNIR data of the Moon and asteroid surfaces, but qualitatively, the thermal effects are outpaced by space-weathering effects.

In the MIR region, thermal gradients will affect remote-sensing spectra of dusty, airless-body surfaces as mentioned above. However, it should be noted that, despite the shifting of the CF and the increased spectral contrast due to large thermal gradients seen in laboratory spectra, the actual positions of the spectral bands remain the same (Donaldson Hanna et al. 2012) and diagnostic. Furthermore, this thermal gradient issue is less of a problem for spectra of coarse particles or rocks, or when the planetary target has an atmosphere that allows interstitial gas conduction and not just grain-to-grain conduction within a particulate medium (Presley & Christensen 1997).

Considering these caveats, once there is an understanding of the how space weathering, the presence or absence of atmosphere, the degree to which temperature gradients affect the surface optical properties over a large wavelength range, etc., planetary data can be cautiously analyzed through comparison to a spectral library of fine-particle mineral samples collected under ambient pressure and temperature conditions, as a starting point for interpreting remote-sensing data.

6. Data Availability Statement

The calibrated, scaled, spliced, and ready-to-use Frankenspectra are all permanently archived at and publicly available in digital format from the NASA Planetary Data System (PDS) Geosciences Node Spectral Library at Washington University in St. Louis.[8] Along with the scaled and spliced Frankenspectra in the Spectral Library, the original laboratory spectra that informed the baseline spectrum in the visible spectral range or provided segments to the Frankenspectra (prior to any scaling) are also available in a separate archive at the PDS. The archive includes all of the measurement parameters for each spectrum. The complete bundle of ready-to-use Frankenspectra and the original laboratory spectra are available on the PDS: doi:10.17189/zshq-d822.

7. Summary

The Frankenspectra of 27 fine-particulate minerals are available through the PDS (https://pds-geosciences.wustl.edu/). These reflectance spectra are openly available to

---

8   https://pds-geosciences.wustl.edu/

researchers who want to use them to analyze spectra of dusty, fine-particulate targets in the solar system. Our multiple-lab approach to measuring the reflectance properties of our samples has enabled us to construct what we believe are the best spectral representations of these fine-particulate samples across the broad far-UV to MIR spectral range of 0.12–20 μm.

ORCID iDs

Melissa D. Lane ● https://orcid.org/0000-0003-3264-3337
Edward A. Cloutis ● https://orcid.org/0000-0001-7301-0929
Roger N. Clark ● https://orcid.org/0000-0002-7021-1220
M. Darby Dyar ● https://orcid.org/0000-0003-4272-793X
Joern Helbert ● https://orcid.org/0000-0001-5346-9505
Amanda R. Hendrix ● https://orcid.org/0000-0002-0435-8224
Gregory Holsclaw ● https://orcid.org/0000-0002-9059-9437
Alessandro Maturilli ● https://orcid.org/0000-0003-4613-9799
Neil Pearson ● https://orcid.org/0000-0002-0183-1581
Mikki Osterloo ● https://orcid.org/0000-0003-3100-4760
Faith Vilas ● https://orcid.org/0000-0003-4723-5870
Daniel Applin ● https://orcid.org/0000-0002-5170-2382

References

Adams, J. B., & McCord, T. B. 1971, Sci, 171, 567
Aronson, J. R., & Emslie, A. G. 1973, ApOpt, 12, 2573
Baldridge, A. M., Hook, S. J., Grove, C. I., & Rivera, G. 2009, RSEnv, 113, 711
Blaney, D. L., & McCord, T. B. 1989, JGR, 94, 10159
Bramble, M. S., Milliken, R. E., & Patterson, W. R., III 2021, Icar, 369, 114251
Byrne, S. A., Dyar, M. D., Bessette, E. E., et al. 2015, LPI, 46, 1499
Christensen, P. R. 1986, JGR, 91, 3533
Clark, R. N., King, T. V. V., Klejwa, M., et al. 1990, JGR, 95, 12653
Donaldson Hanna, K. L., Wyatt, M. B., Thomas, I. R., et al. 2012, JGRE, 117, E00H05
Gayk, T., & Kleinschrodt, R. 2000, JMetG, 18, 293
Hallatt, D., Leroux, H., & Roussel, P. 2021, LPSC, 52, 2518
Hendrix, A. R., & Vilas, F. 2006, AJ, 132, 1396
Hinrichs, J. L., & Lucey, P. G. 2002, Icar, 155, 169
Kokaly, R. F., Clark, R. N., Swayze, G. A., et al. 2017, USGS Spectral Library Version 7 Data Series 1035, USGS doi:10.3133/ds1035
Lane, M. D., & Christensen, P. R. 1998, Icar, 135, 528
Lantz, C., Binzel, R. P., & DeMeo, F. E. 2017, Icar, 302, 10
Logan, L. M., & Hunt, G. R. 1970, JGR, 75, 6539
Lyon, R. J. P. 1964, Evaluation of Infrared Spectrophotometry for Compositional Analysis of Lunar and Planetary Soils. II. Rough and Powdered Surfaces NASA CR-100, NASA, https://ntrs.nasa.gov/citations/19650001173
Masiero, J., Hartzell, C., & Scheeres, D. J. 2009, AJ, 138, 1557
McKay, D. S., Heiken, G., Basu, A., et al. 1991, Lunar Sourcebook: A User's Guide to the Moon (Cambridge: Cambridge Univ. Press), 285
Mustard, J. F., & Hays, J. E. 1997, Icar, 125, 145
Pieters, C. M. 1986, RvGeo, 24, 557
Pieters, C. M., Fischer, E. M., Rode, O., & Basu, A. 1993, JGR, 98, 20817
Presley, M. A., & Christensen, P. R. 1997, JGR, 102, 6535
Ruff, S. W., & Christensen, P. R. 2002, JGRE, 107, 5127
Salisbury, J. W., & Eastes, J. W. 1985, Icar, 64, 586
Shelley, M. 1818, Frankenstein; or, The Modern Prometheus (London: Lackington, Hughes, Harding, Mavor, & Jones)
Shirley, K. A., & Glotch, T. D. 2019, JGRE, 124, 970
Vincent, R. K., & Hunt, G. R. 1968, ApOpt, 7, 53